JCTC Journal of Chemical Theory and Computation

Article

Cite This: J. Chem. Theory Comput. 2019, 15, 938−948

pubs.acs.org/JCTC

Meeting the Challenge of Magnetic Coupling in a Triply-Bridged Chromium Dimer: Complementary Broken-Symmetry Density Functional Theory and Multireference Density Matrix Renormalization Group Perspectives

Dimitrios A. Pantazis*

Max-Planck-Institut für Kohlenforschung, Kaiser-Wilhelm-Platz 1, 45470 Mülheim an der Ruhr, Germany

Supporting Information

ABSTRACT: Face-sharing octahedral dinuclear Cr(III) compounds with d^3−d^3 electronic configurations represent nontrivial examples of electronic complexity, posing particular challenges for theoretical and computational studies. A tris-hydroxy-bridged Cr(III)−Cr(III) system has proven to be a richly rewarding target for studies of magnetism and electron paramagnetic resonance spectroscopy. It was also reported to be a peculiarly difficult system to treat with density functional theory (DFT). In this work the magnetic coupling problem for this dimer is approached with broken-symmetry (BS)-DFT and multireference calculations that utilize the density matrix renormalization group (DMRG) to handle full-valence active spaces. BS-DFT is shown to recover the correct ordering and energy spacing of Heisenberg spin states if used in conjunction with appropriate spin projection procedures, albeit with pronounced functional sensitivity. The contrasting conclusions of previous studies are traced to incorrect inclusion of electronically excited configurations. Analysis of the direct and differential overlap of corresponding orbital pairs from the BS-DFT solution indicates that metal−metal through-space interaction is the dominant contributor to antiferromagnetic coupling. At the DFT level a procedure that utilizes pseudopotential substitution is demonstrated that allows evaluation of the direct exchange vs superexchange contributions. A complementary description is obtained with DMRG-SCF calculations that enable state-averaged CASSCF calculations with both metal and bridge orbitals in the active space. A localized orbital subspace analysis supports the DFT conclusions that in contrast to doubly bridged isoelectronic analogues, antiferromagnetic coupling in the chromium dimer arises primarily from direct metal−metal interaction but is significantly enhanced by ligand-mediated superexchange.

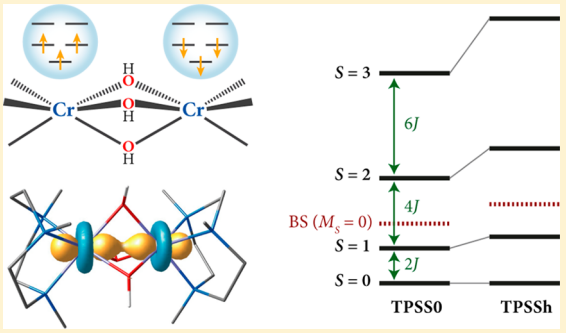

1. INTRODUCTION

Dinuclear complexes of open-shell transition metal ions are archetypal systems in the field of molecular magnetism.[1] Properties related to the low-energy region of their electronic states spectrum are typically discussed using the model of effective magnetic interactions. Associated semiempirical concepts derived from phenomenological approaches, such as direct exchange and superexchange, are employed to rationalize the observed ferromagnetic or antiferromagnetic coupling and systematize experimental data. Quantum chemistry contributes greatly to the analysis of exchange coupled systems by exploring and establishing connections between observable properties, phenomenological parameters, and the electronic structure.[2−4] A question that arises in most investigations of exchange coupled systems concerns the pathways by which the interaction between the spin sites is "mediated". In the case of complexes where the metal ions are separated by a linear bridging ligand, it is clear that no "direct" metal−metal interaction can be established. Doubly bridged dimers, for example bis-μ-oxo complexes, typically fall in the same category, with low-spin ground states (antiferromagnetic coupling) considered to arise from Anderson ligand-mediated superexchange.[5,6] However, in multiply bridged dimers the situation becomes less clear-cut because the bridging topology can often bring the metal ions in close proximity and the antiferromagnetic coupling may be stronger than expected from the chemical nature of the bridges compared with the interaction they supposedly mediate in doubly bridged analogues. The dinuclear copper acetate dehydrate is a classic example of ambiguities that arise in the description of the "antiferromagnetic magnetic interaction", with proposed interpretations ranging from weak direct Cu−Cu bonding to the currently accepted acetate-mediated superexchange.[7,8]

Chromium(III) dimers constitute a class of antiferromagnetically coupled systems that has given rise to considerable ambiguities and debates regarding the most appropriate description of their magnetic properties. The idea of direct

Received: September 25, 2018
Published: January 15, 2019

DOI: 10.1021/acs.jctc.8b00969
J. Chem. Theory Comput. 2019, 15, 938−948

exchange was initially dismissed, and the magnetic interaction between the Cr(III) ions was attributed to ligand-mediated superexchange.[9] However, a clear trend was eventually established based on empirical data, showing that in face-sharing octahedral Cr(III) dimers the strength of antiferromagnetic coupling correlates well with the metal−metal distance. Niemann et al.[10] therefore proposed the diametrically opposite thesis that through-space interaction is the only mechanism responsible for antiferromagnetic coupling in face-sharing octahedral d^3−d^3 complexes of V(II), Cr(III), and Mn(IV), because the metal−metal distance appeared to be the only relevant structural parameter for the exchange coupling constants.

Tris-hydroxo-bridged Cr(III) dimers, such as the series $[L_2Cr(III)_2(\mu\text{-}OH)_3]^{+3}$ (L = *N,N′,N″*-trimethyl-1,4,7-triazacyclononane, Figure 1)[9−12] that have been crystallized with a

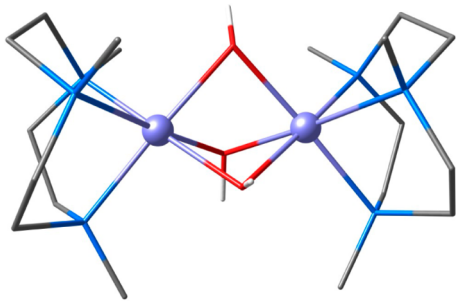

Figure 1. Chromium dimer $[L_2Cr(III)_2(\mu\text{-}OH)_3]^{+3}$, L = *N,N′,N″*-trimethyl-1,4,7-triazacyclononane.

variety of counterions, are representative examples of such dimeric Cr(III) systems that continue to generate interest owing to their magnetic properties and remarkable electron paramagnetic resonance (EPR) spectroscopic features.[12−14] From the point of view of quantum chemistry, a particularly intriguing aspect is the reported inability of density functional theory (DFT) to describe the basic features of the antiferromagnetic coupling in the Cr(III) dimers even at a qualitative level.[13] If DFT fails to describe the magnetic coupling in these complexes, then the fundamental question of distinguishing between the conflicting models of magnetic coupling (direct exchange vs ligand-mediated superexchange) would remain in principle inaccessible to DFT.[13,14] On the other hand, the cost of high-level multireference methods such as difference-dedicated configuration interaction (DDCI)[15,16] renders them impractical or inapplicable for systems with multiple unpaired electrons and orbitals in the active space, particularly because of the need to include high-order excitations.[3,17,18]

In recent years an enormous body of work has been published on the DFT treatment of exchange coupling in transition metal complexes using the broken-symmetry DFT approach (BS-DFT),[19−27] while other DFT-based approaches are being pursued.[28−32] BS-DFT studies on exchange-coupled chromium complexes are scarce but indicate that the approach performs satisfactorily.[33−37] Numerous BS-DFT studies for electronically related high-valent manganese complexes[38−50] (the Cr(III) ion has the same electron configuration, d^3, and local spin, $S = 3/2$, as the Mn(IV) ion) have reported very good results in terms of exchange coupling constants to the point that it has been claimed that BS-DFT correctly reproduces the experimentally established ground spin states of all known structurally characterized complexes that contain Mn(III) and Mn(IV) ions.[48] In view of these successes, it is puzzling that the method was reported to fail spectacularly for the title Cr(III) dimer.[13]

In addition to a long series of successful applications of BS-DFT, the density matrix renormalization group (DMRG)[51−54] has recently enabled the first applications of complete active space self-consistent field (CASSCF) and *N*-electron valence perturbation theory (NEVPT2)[55−58] calculations to dinuclear exchange-coupled transition metal complexes using unprecedent numbers of active electrons and orbitals.[59−61] The use of extended CAS specifically attempts to take explicitly into account excitations that would otherwise have to be treated with a method such as DDCI. These recent achievements suggests that the problem of the Cr(III) dimers could also be approached with multireference methods using active spaces much larger than the metal-only active space already covered in previous CASSCF studies.[13]

In the present work the magnetic coupling in the archetypal tris-μ-hydroxo Cr(III) dimer shown in Figure 1 is examined from the complementary perspectives of broken-symmetry DFT and multireference wave function theory employing DMRG-driven CASSCF calculations (DMRG-SCF). A detailed exposition of the applied BS-DFT procedure is presented. The results demonstrate that the magnetic coupling in the Cr(III) dimer can be correctly described by DFT, both qualitatively and quantitatively, provided the broken-symmetry approach is properly applied in combination with spin projection techniques and that the intrusion of irrelevant excited electronic configurations is avoided. Based on the present results, the conclusions of previous studies[13] are thoroughly revised. In addition, the nature of the spin coupling in the complex is studied using two approaches: one based on the Amos−Hall corresponding orbital transformation of broken-symmetry DFT solutions[62,63] and the other based on DMRG-SCF calculations in which the active space encompasses successive orbital subspaces localized on distinct units of the complex. Both approaches show that the spin coupling in the Cr dimer is dominated by direct through-space interaction between the Cr ions. However, both methods also suggest that superexchange plays an important ancillary role in enhancing the antiferromagnetic coupling.

2. COMPUTATIONAL DETAILS

The crystallographic coordinates for the chromium dimer were obtained from the structure deposited at the Cambridge Structural Database with Refcode BIHYUM, which corresponds to $[L_2Cr(III)_2(\mu\text{-}OH)_3]I_3{\cdot}3H_2O$.[9,11,12] In preparing the model all counterions and crystallization waters were removed. Where present, hydrogen atoms were also removed and reintroduced manually. As a first step in the computational treatment, geometry optimizations were performed in which all heavy atoms were fixed to their crystallographic positions, but all hydrogen atoms were allowed to be fully optimized. Geometry optimizations utilized the TPSS functional[64] with D3BJ dispersion corrections[65,66] and def2-TZVP basis sets for all atoms.[67] The resolution of the identity (RI) approximation was employed for fitting the Coulomb integrals, in combination with the auxiliary basis sets of Weigend (def2/J).[68] All calculations were performed with ORCA[69] using increased integration grids (Grid5) and tight SCF convergence criteria. Subsequently, single point calculations were performed with various functionals to obtain final energies of the high-

DOI: 10.1021/acs.jctc.8b00969
J. Chem. Theory Comput. 2019, 15, 938−948

spin and the broken-symmetry states. The FlipSpin feature of ORCA was used to generate the initial guess for the BS calculation. The chain of spheres approximation to exact exchange (COSX)[70] was used for hybrid functionals with increased integration grids (GridX7). Convergence to the desired BS solution was confirmed by inspection of orbitals and spin populations. The energy difference between the high-spin and broken-symmetry solutions along with their spin expectation values $\langle S^2 \rangle$ were used in the Yamaguchi formula[71] to extract the exchange coupling constant as

$$J = -\frac{E_{HS} - E_{BS}}{\langle S^2 \rangle_{HS} - \langle S^2 \rangle_{BS}}$$

Multireference calculations (CASSCI and CASSCF) were performed with ORCA,[69] using the interface with the BLOCK code[51,72−75] for calculations that utilized the DMRG algorithm. Initial orbitals for multireference calculations were obtained by localization of quasi-restricted[76] DFT orbitals using the Pipek−Mezey localization algorithm.[77] The active space used in multireference calculations is indicated as ($N_{electrons}$, $N_{orbitals}$). Auxiliary basis sets by Hättig[78] were employed in parts of the calculations that made use of the RI approximation. Orbital optimization with CASSCF and DMRG-SCF was performed in a state-averaged manner unless otherwise indicated in the text, i.e. the orbitals were simultaneously optimized for all states of the spin ladder. In DMRG-SCF calculations the orbitals were automatically reordered with the Fiedler algorithm to optimize convergence behavior.[79−82] The number of retained states M in the renormalization step of DMRG calculations was increased until the relative energies of all spin states computed by DMRG-SCF were converged to wavenumber (cm^{-1}) accuracy. Calculations employing the N-electron valence perturbation theory (NEVPT2)[55,57] were also performed for selected active spaces with both the strongly contracted and fully internally contracted (also known as partially contracted) variants of the method.

3. RESULTS AND DISCUSSION

3.1. Exchange Coupling Constants from Broken-Symmetry DFT. The two d^3 Cr(III) ions have local spins $\mathbf{S}_A$ and $\mathbf{S}_B$ with $S_A = S_B = 3/2$. Their coupling leads to a series of states with total spin $S = S_A + S_B, S_A + S_B - 1, \ldots, |S_A - S_B|$, specifically four states with $S = 3$, 2, 1, and 0. Their order and spacing can be modeled by the isotropic Heisenberg−Dirac−van Vleck Hamiltonian

$$H_{HDvV} = -2J\mathbf{S}_A\mathbf{S}_B$$

where J is the exchange coupling constant that parametrizes the fictitious exchange interaction, negative for antiferromagnetic and positive for ferromagnetic coupling. Additionally, small deviations from the ideal spacing of spin states can be modeled by inclusion of a biquadratic term $j(\mathbf{S}_A\mathbf{S}_B)^2$, a minor perturbation that has been occasionally employed in the fitting of experimental data but will not be considered in the present work. According to the above Hamiltonian, the energies of the four spin states are given by the Landé formula

$$E(S) = -J[S(S+1) - S_A(S_A+1) - S_B(S_B+1)]$$

and hence the spin states are spaced by $2J$ ($S = 0$ to $S = 1$), $4J$ ($S = 1$ to $S = 2$), and $6J$ ($S = 2$ to $S = 3$), yielding a total energy span of $12J$ for the spin ladder. Experimentally the exchange coupling constant J for the chromium complex discussed here was fitted to a value of -66 cm^{-1}.[10]

Of the four spin states only the ferromagnetic $S = 3$ state can be approximated with a single determinant and hence is the only state that can be computed directly with Kohn−Sham DFT. To compute the energies of all other states one has to rely on the broken-symmetry approach, whereby an unrestricted determinant is constructed by breaking the spatial symmetry of the spin manifolds and allows the singly occupied orbitals to localize on the two distinct spin sites with opposite spins. This BS determinant is not an eigenfunction of the $\mathbf{S}^2$ spin operator and does not correspond to any of the spin states discussed above. It is not characterized by a spin quantum number S (it can however be considered a mixture of spin states)[83] but only by a magnetic quantum number M_S. In the present case, the BS solution is obtained by allowing the six singly occupied molecular orbitals to localize on the two metal ions with three unpaired electrons of α spin on one Cr and three unpaired electrons of β spin on the other (total $M_S = 0$). A single geometry derived from the experimental crystal structure is used in all calculations. When an experimental geometry is not available, then DFT optimizations are often carried out using either the high-spin or the broken-symmetry solution, but it is noted that the "extended broken-symmetry" approach in principle enables access to the symmetry-reconstructed spin surface in cases when this is required.[43,84−86]

It is crucial in these calculations to preserve the local S_z components, which poses two fundamental requirements for the approach to be meaningful: 1) the number of effectively unpaired electrons on each site must be identical in the HS and BS solutions, and 2) all unpaired electrons on a given metal site must be of the same spin.[87] Convergence to the desired BS solution can be confirmed by inspection of atomic spin populations. The correct solution has the same number of unpaired electrons as the ferromagnetic HS state, i.e. three unpaired electrons on each Cr center, but one of the ions carries negative (β) spin.

For every density functional used in the present study, the spin populations of the Cr ions in the BS solutions were ca. +2.9 and −2.9 electrons, close to the formal integer count. This confirms that the correct BS solution was obtained. It is noted that the atoms of the bridging ligands have negligible spin populations; therefore, the spins are well-defined, and the HDvV Hamiltonian can be applied without complications. The energy difference between the high-spin $S = 3$ and the BS state ($E_{HS} - E_{BS}$) and the $\langle S^2 \rangle$ expectation value of each solution were used in the Yamaguchi formula[71] to deduce the exchange coupling constant J. This value was used in the Landé formula to obtain the energies of the three spin states that cannot be computed directly, i.e. the $S = 0$, $S = 1$, and $S = 2$ states.

Given that the strength of exchange coupling predicted by BS-DFT is known to be dependent on the percentage of Hartree−Fock (HF) exchange, we tested a sequence of functionals that build on the same parent method but include increasing HF exchange: TPSS (no HF exchange), TPSSh (10% HF exchange),[88] and TPSS0 (25% HF exchange). All computed quantities for these and additional functionals are listed in Table S1. It is noted that TPSSh has been shown to provide accurate exchange coupling constants for high-valent manganese systems, which is important because Mn(IV) is isoelectronic with Cr(III). As reported repeatedly for non-hybrid functionals, the computed TPSS value for J (−113.8

DOI: 10.1021/acs.jctc.8b00969
J. Chem. Theory Comput. 2019, 15, 938−948

cm^{-1}) is significantly overestimated compared to the experimental value of −66 cm^{-1}. TPSSh reduces the exchange coupling constant to −84.8 cm^{-1}, and TPSS0 reduces it further to −61.3 cm^{-1}. These two hybrid functionals thus bracket the experimental value of −66 cm^{-1}, with the higher percentage of HF exchange yielding closer agreement with experiment. For comparison with another popular method, B3LYP (20% HF exchange)[89,90] leads to J = −74.3 cm^{-1}. The "optimal" percentage of HF exchange is therefore slightly higher than that determined for Mn systems,[41,42,47] in line with the observations of Morsing et al.[34] Figure 2 summarizes the BS-DFT results, showing the energy of the BS solution with respect to the projected spin states. In practice the $\langle S^2 \rangle$ expectation values for the high-spin and broken-symmetry solutions are close to 12 and 3, respectively (see Table S1), so the $E_{HS} - E_{BS}$ energy difference is approximately 9J.

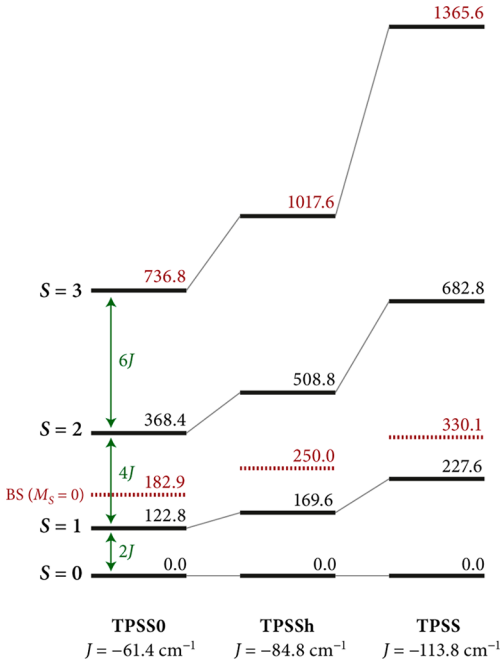

Figure 2. Spin ladders produced by three different functionals for the dinuclear chromium complex under investigation. The relative energies of spin states are deduced from the exchange coupling constant obtained by broken-symmetry DFT and the Yamaguchi projection using the Landé formula. The relative energies of the broken-symmetry solutions (dotted lines) are indicated for each functional.

Table S2 reports geometric parameters and exchange coupling constants for structures that were fully optimized using a series of functionals. Compared to the crystallographic model all functionals predict longer Cr−Cr distances in the gas phase (by 0.05 Å for TPSS and up to 0.09 Å for B3LYP) as the effects of crystal packing are eliminated. The Cr−O(H) bond lengths also appear slightly longer, by ca. 0.02 Å on average. In line with these changes all functionals yield lower values for the exchange coupling constant, although GGA functionals still overestimate the strength of antiferromagnetic coupling. When optimized structures are used, TPSSh is closest to the experimental value, with a predicted exchange coupling constant J = 56.0 cm^{-1} (see Table S2). In conclusion, apart from the anticipated dependence of the $E_{HS} - E_{BS}$ gap on the nature of the functional, BS-DFT affords a perfectly reasonable description of this Cr(III) dimer.

3.2. Analysis of the Broken-Symmetry Solution. A way of analyzing the unrestricted broken-symmetry wave function is in terms of "corresponding orbitals".[4,62,63] The corresponding orbital transformation this leads to has maximally similar α and β orbital pairs, i.e. pairs where the α and β orbitals have overlap close to unity forming an approximately closed-shell manifold, plus a set of α and β orbitals that typically have distinct spatial parts localized on different parts of the molecule with pairwise overlap integrals significantly lower than one. These orbitals, which describe the unpaired electrons of the system, resemble the "magnetic orbitals" in nonorthogonal orbital treatments of molecular magnetism.[1] In exchange coupled systems the regions of overlap for these corresponding orbital pairs reveal the (super)exchange pathways. The greater their overlap integral, the more the specific pair or pathway contributes to antiferromagnetic coupling.

The results of the corresponding orbital transformation for the present system are shown in Figure 3. Of the three corresponding orbital pairs the most important type of interaction is of a direct metal−metal type (orbital pair 129). The orbitals of the strongly interacting pair resemble chromium d_{z^2} orbitals with a σ-type overlap. Therefore, the coordination geometry of each Cr ion is best viewed as distorted trigonal prismatic (Figure 4) and hence the frame of the molecule as composed of two such prisms joined along the z axis at the three shared bridging OH groups. The other two corresponding orbital pairs (130α/β and 131α/β in Figure 3), which relate to the d_{xy} and $d_{x^2-y^2}$ orbitals of the chromium ions, present the same overlap, which is considerably smaller than that of the d_{z^2} orbitals but nonzero. In the case of these e′ parentage corresponding orbital pairs, overlap apparently can only occur over the bridges. It is noted that the orbitals of all pairs have delocalization tails on the bridging groups, including pair 129. Even though it is not possible to quantify the contribution of different pathways based on this analysis, from the relative overlaps of the three pairs it could be surmised that

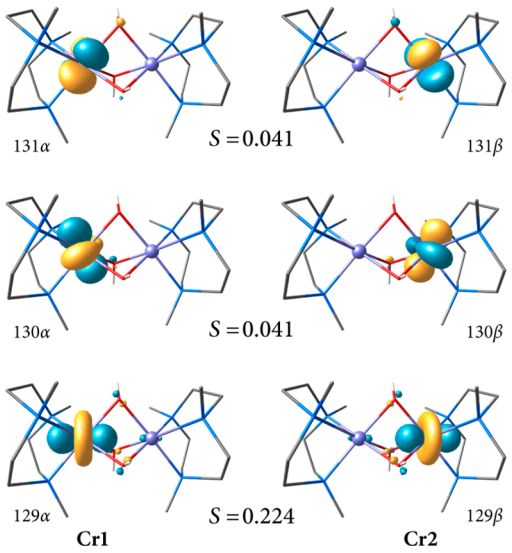

Figure 3. Pairs of "magnetic orbitals" derived from the corresponding orbital transformation of the broken-symmetry DFT determinant (the TPSSh solution was used here). The S values here indicate the values of overlap integrals for the corresponding pairs.

DOI: 10.1021/acs.jctc.8b00969
J. Chem. Theory Comput. 2019, 15, 938−948

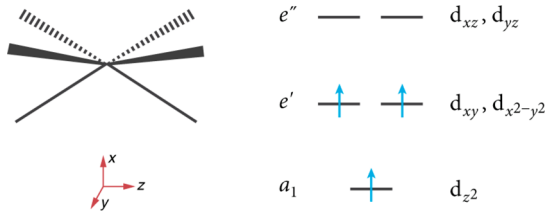

Figure 4. Idealized trigonal prismatic coordination geometry (D_{3h} point group) with schematic d orbital splitting. The reduced symmetry in the real dimer does not affect significantly the d_{z^2} orbitals of the two Cr(III) ions that remain nonbonding with respect to the ligands and available for "through-space" metal−metal interaction.

OH-mediated superexchange does not play a major role in the stabilization of the antiferromagnetic ground state of the dimer.

3.3. Evaluation of Previous DFT Results. The results presented above show that the broken-symmetry DFT approach leads to the correct description of the exchange coupling constant in the chromium dimer, predicting antiferromagnetic coupling of the same order of magnitude as the experimentally determined value and allowing a qualitative interpretation in terms of the corresponding orbital transformation. Even though quantitative reproduction of the experimentally fitted constant has to rely on empirical functional selection, the ladder of magnetic (Heisenberg) spin states resulting from the coupling of the two $S = 3/2$ Cr(III) ions is correctly reproduced regardless of the choice of method. These conclusions contrast strongly with a previous study by Bennie et al.,[13] who suggested that DFT fails dramatically for this chromium dimer and reported irregular non-Heisenberg ordering of states, with $S = 0$ as the ground state followed by $S = 3$ within a few hundred wavenumbers (912 cm^{-1} with the B3LYP functional) and the $S = 2$ and $S = 1$ states close together (135 cm^{-1} with B3LYP) but far removed from the $S = 0$ and $S = 3$ states by several *thousands* of wavenumbers (more than 7300 cm^{-1} with B3LYP).[13] Since this type of ordering and spacing of spin states is hard to rationalize and would represent an unprecedented failure for DFT, it is crucial to understand what is the root cause of these strongly contrasting conclusions.

The answer is already present in the original data published by Bennie et al., specifically in the reported Mulliken spin populations for the various DFT solutions (Table 1 of that paper).[13] It is clear that the high-spin, ferromagnetic $S = 3$ state was correctly computed, with local high-spin configurations of the Cr(III) ions reflected in the spin populations close to the value of 3. A lower-energy broken-symmetry $M_S = 0$ state was also computed as shown by the spin populations of ca. 3 on one center and −3 on the other. The energy difference between these states reported with the B3LYP functional (912 cm^{-1}) is similar to the energy differences between high-spin and broken-symmetry solutions obtained in the present work (Table S1). If this is assumed to be approximately equal to 9J, then the exchange coupling constant would be ca. 101 cm^{-1}. Crucially, this broken-symmetry $M_S = 0$ solution was not recognized as such but was incorrectly (see Figure 2) designated as a $S = 0$ state. That is, the high-spin and broken-symmetry solutions were not used in a spin projection procedure to derive the exchange coupling constant of the dimer, from which to deduce the correct energy—within the limits of the Heisenberg Hamiltonian—of the antiferromagnetic $S = 0$ state, but rather the BS solution was regarded as a spin eigenfunction and its energy incorrectly equated with the experimentally observed ground state of the complex.

Given that the exchange coupling constant was not determined, it is perplexing how the energies of the intermediate spin states with $S = 1$ and $S = 2$, by definition inaccessible through single-determinant DFT calculations, were obtained in ref 13. The answer is again to be found in the reported spin populations.[13] Presumably an attempt was made to compute the energies of these states *directly*, by setting the multiplicity of the system to 3 and 5, respectively, and running a Kohn−Sham calculation under this restriction. This resulted in *pairing* of electrons within one of the Cr ions, most likely in the d_{z^2} orbital, as revealed by the spin populations of ca. 1 electron in the solution reported as "$S = 2$" and of ca. −1 electron in the solution mislabeled as "$S = 1$", which is but the broken-symmetry version of the former. Therefore, these results simply reflect the energy of a spin-forbidden ligand-field transition, i.e. the energy required to switch the electronic configuration of one Cr(III) ion from a high-spin d^3 spin-quartet to a low-spin d^3 spin-doublet configuration. However, these low-spin paired-electron configurations are irrelevant for the magnetic coupling problem of two $S = 3/2$ ions: they represent excited electronic configurations far removed from the ground state manifold of magnetic levels. Unsurprisingly, therefore (but correctly in a *technical* sense), these spin-paired solutions (mislabeled as $S = 1$ and $S = 2$ states but actually $M_S = 1$ and $M_S = 2$ BS determinants of an excited electronic configuration) were reported to lie thousands of wave numbers above the ferromagnetic $S = 3$ state that defines the topmost rung of the Heisenberg spin ladder for the ground-state electronic configuration. Equally unsurprisingly, attempts to deduce EPR parameters with DFT on the basis of these high-energy excited electronic configurations led to results that could not be meaningfully compared with experiment,[13] because these solutions are either unphysical or do not represent states accessible to EPR spectroscopy.

In conclusion, beyond the well-known functional sensitivity, there is nothing particularly problematic about the performance of DFT for the present chromium dimer system. Previous reports to the contrary were sidetracked by the neglect of spin projection techniques and by electronic structure solutions unrelated to the magnetic coupling problem of two $S = 3/2$ spins. The high energetic penalty for electron-pairing led to broken-symmetry solutions much higher in energy than even the highest-energy ferromagnetic state of the ground electronic configuration of the dimer, creating the illusion of spin-state inversion.[13] In general, it can be suggested that studies which reportedly target intermediate spin states of exchange-coupled systems directly with simple DFT calculations should be treated with caution because this task is by definition impossible with a collinear-spin approach. Reports of suspiciously large errors for the relative energies of intermediate spin states, of a magnitude much larger than the expected exchange coupling constant but similar to that of ligand-field transitions,[13,91] should be carefully scrutinized because such calculations likely report on excited electronic configurations of no direct relevance to the magnetic coupling problem. The related problem of computing magnetic properties (such as local zero-field splitting and hyperfine coupling tensors) with DFT for low-spin states of exchange-coupled systems has been partially addressed through the use of spin projection techniques.[4,41,42,47,92−96]

DOI: 10.1021/acs.jctc.8b00969
J. Chem. Theory Comput. 2019, 15, 938−948

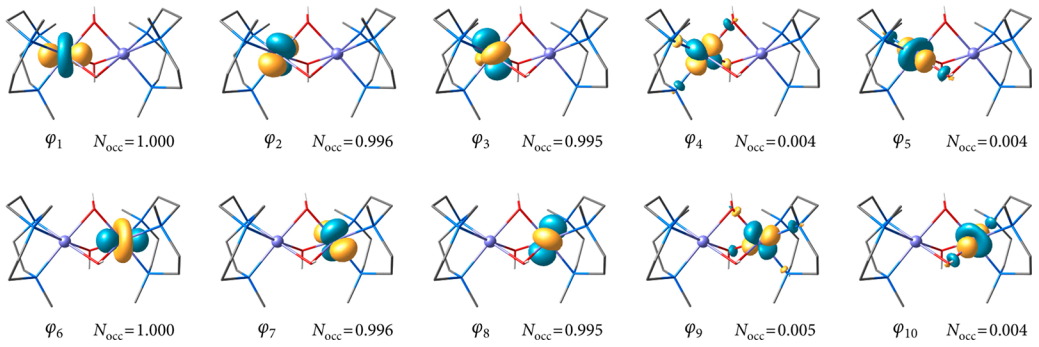

Figure 5. Localized orbitals from state-averaged CASSCF calculations with a (6e,10o) active space and their occupation numbers.

3.4. CASSCF Calculations with Metal-Only Active Space. Multireference calculations allow direct access to all spin states without the need for spin projection approximations. In this section we discuss a basic CASSCF treatment of the system. An active space composed of the ten 3d orbitals of the Cr ions was constructed for CASSCF calculations. Localized orbitals were used to enable a more intuitive reading of the results in terms of local electronic configurations and as the basis for DMRG calculations that will be discussed in the following. To avoid possible spurious deviations from Heisenberg behavior,[61] state-averaged orbital optimization was employed over all four spin states, with equal weights for all states. The CASSCF (6e,10o) calculations produce a normal Heisenberg ordering of states as that reported previously,[13] with the antiferromagnetic $S = 0$ state being the lowest in energy, 32.9 cm^{-1} below the $S = 1$ state. The $S = 2$ state is at 99.5 cm^{-1}, and the ferromagnetic $S = 3$ state is at 201.9 cm^{-1}. State-averaged CASSCF calculations reported by Bennie et al. have a wider spacing of states, suggestive of greater stabilization of low-spin states. On the other hand, the spacing of states in the present study follows a regular Landé pattern, justifying the extraction of a single average exchange coupling constant ($J = -16.8$ cm^{-1}). This is in contrast to the state-averaged CASSCF results of Bennie et al., which showed irregular spacing of successive spin states with either contraction or expansion of the spin ladder at higher S values depending on the basis set used.[13] It is not possible to clarify the origin of this behavior in ref 13, which is unexpected for state-averaged calculations,[61,97] but both studies agree that CASSCF (6e,10o) calculations significantly underestimate the antiferromagnetic coupling.

Focusing first on qualitative aspects, Figure 5 depicts localized CASSCF state-averaged orbitals and their natural occupation numbers. The strongly occupied orbitals (Figure 5) are highly similar to the corresponding orbitals of the broken-symmetry DFT calculations—although not equivalent due to orthogonality—and confirm the qualitative magnetic orbital picture discussed above (Figure 3).

For each one of the four spin states computed by CASSCF calculations the weight of the [11100 11100] configuration (the notation follows the listing of orbitals shown in Figure 5) exceeds 98%. The dominance of this configuration is also clear from the natural occupation numbers shown in the same figure, which deviate only slightly from zero for orbitals of e″ parentage. This is in line with the view that magnetic coupling is a multideterminantal but not intrinsically a multiconfigurational problem. It is instructive to see how this given configuration leads to the different total spin states, and this can be made transparent by casting the solutions in terms of a linear combination of spin determinants. Approximating the occupations of the e″ parentage orbitals as zero, the ferromagnetic $S = 3$ state can be represented by a unique high-spin determinant, $|\varphi_1\varphi_2\varphi_3\varphi_6\varphi_7\varphi_8|$, and then the $S = 2$ state is a linear combination of six $M_S = 2$ determinants obtained by a single spin flip, within one and the same orbital configuration: $|\bar{\varphi}_1\varphi_2\varphi_3\varphi_6\varphi_7\varphi_8|$, $|\varphi_1\varphi_2\varphi_3\bar{\varphi}_6\varphi_7\varphi_8|$, $|\varphi_1\bar{\varphi}_2\varphi_3\varphi_6\varphi_7\varphi_8|$, $|\varphi_1\varphi_2\varphi_3\varphi_6\bar{\varphi}_7\varphi_8|$, $|\varphi_1\varphi_2\bar{\varphi}_3\varphi_6\varphi_7\varphi_8|$, and $|\varphi_1\varphi_2\varphi_3\varphi_6\varphi_7\bar{\varphi}_8|$. Similarly, the $S = 1$ state can be written as a combination of 15 spin determinants with $M_S = 1$, i.e. two spin flips with respect to the high-spin determinant, and finally the antiferromagnetic $S = 0$ state as a linear combination of 20 determinants with $M_S = 0$. One of these $M_S = 0$ determinants resembles in spin alignment the broken-symmetry Kohn−Sham determinant, i.e. $|\varphi_1\varphi_2\varphi_3\bar{\varphi}_6\bar{\varphi}_7\bar{\varphi}_8|$, but obviously without equivalence in the spatial orbital part.

Although this analysis explains the fundamental multideterminantal nature of spin coupling, the minimal active space CASSCF(6e,10o) calculations are insufficient to quantitatively reproduce the magnitude of the exchange coupling. The spin state ladder is qualitatively correct and very close to a regular Landé pattern, but the antiferromagnetic exchange coupling constant (average $J = -16.8$ cm^{-1}) is approximately one-fourth of the experimental value, and hence the spin ladder is compressed compared to experiment. Underestimation of the antiferromagnetic interaction in transition metal dimers by CASSCF calculations that involve only metal d orbitals is a well-known fact, attributable to the inability of the small active space to capture the physics of the spin coupling and the inability of the method to recover dynamic electron correlation.[3]

It is important however to place these numbers in context. In a bis-μ-oxo/μ-acetato manganese dimer[98] studied recently with multireference methods and which exhibits antiferromagnetic coupling of similar magnitude (−90 cm^{-1}) to the present chromium system, CASSCF calculations with a metal-only active space only marginally registered the presence of an antiferromagnetic interaction (average $J = -1.6$ cm^{-1}).[61] It was only upon inclusion of orbitals of the bridging ligands that antiferromagnetic exchange was "switched on", leading to an exchange coupling constant of almost −60 cm^{-1}. Similar results, i.e. absence of significant coupling at the CASSCF level when using an active space composed only of the "magnetic" orbitals accommodating the unpaired electrons or only of metal d orbitals, have been reported for various other systems. In view of these results, what is truly surprising in the present case of the chromium dimer is that the antiferromagnetic

DOI: 10.1021/acs.jctc.8b00969
J. Chem. Theory Comput. 2019, 15, 938−948

exchange predicted by CASSCF using a metal-only active space is unexpectedly *large* for the method.

If such a substantial portion of the exchange interaction is already captured without including ligand orbitals in the active space, this is a strong indication that the complex exhibits direct Cr−Cr interaction, corroborating the conclusions from the corresponding orbital analysis. Maintaining the minimal active space, improvement of the value in absolute terms can be achieved through methods that include dynamic correlation. As a test we applied NEVPT2 on the (6e,10o) CASSCF solution, and this led to doubling of the magnitude of the exchange coupling constant to −31.8 cm^{-1} (−35.3 cm^{-1} for the fully internally contracted NEVPT2, see Figure S1). Given that our focus in this work is on better understanding the nature of the magnetic coupling in this complex, we will not further pursue ways of attaining numerically satisfying results with multireference methods. It is possible that larger active spaces,[3,61,99,100] higher-order methods,[3] or likely both would be required to achieve quantitative reproduction of experiment.

3.5. Nature of the Antiferromagnetic Coupling. The mechanism of spin coupling in face-sharing d^3−d^3 dimers has been controversially discussed in the literature, with some authors supporting direct metal−metal interaction and others supporting bridge-mediated superexchange. The results presented here for the chromium dimer, both from broken-symmetry DFT and from CASSCF calculations, are consistent with the suggestion that through-space interaction ($d_{z^2} - d_{z^2}$) and not ligand-mediated superexchange is responsible for the antiferromagnetic coupling. However, a more nuanced picture of the coupling emerges via further analysis.

An important question regarding the modulation of the antiferromagnetic coupling concerns the precise effect of the Hartree−Fock exchange in the density functional. All functionals predict direct metal−metal interaction to be the main driver of antiferromagnetic coupling (see above), but it was observed that varying the HF exchange within a given type of density functional correlates systematically with variation of the computed exchange coupling constant from BS-DFT. We proceed with the assumption that the enhancement of antiferromagnetic exchange afforded by decreasing the percentage of HF exchange in the functional may be the result of a physically meaningful enhancement of the actual exchange mechanism. In this case, by analyzing not the corresponding orbital pairs directly but their *differences* for a pair of functionals it is possible to gain insight into the modulation of pathways responsible for the coupling. Taking the difference between the squares of summed corresponding orbital pairs the resulting picture (see Figure 6 for a comparison between TPSSh and TPSS0) clearly suggests that the corresponding orbital pairs from two functionals with different HF exchange differ almost exclusively in the contribution of *bridge* orbitals to the strongly overlapping corresponding orbital pair. In other words, different HF percentages predict different strengths of the spin coupling principally not by modulating the main (direct) interaction pathway but by adjusting an ancillary mechanism, that of bridge-mediated superexchange.

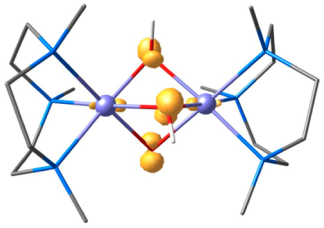

Figure 6. Squared difference between TPSSh and TPSS0 for the strongly overlapping corresponding orbital pair 129 of Figure 3. The lower percentage of HF exchange in TPSSh compared to TPSS0 mostly enhances the contribution of the bridging ligands.

A possible approach to disentangle the contributions of direct exchange and superexchange in the framework of broken-symmetry DFT is to effectively remove from the calculation the orbitals of the bridging ligands that can participate in superexchange. This was attempted here by replacing each OH^- bridge by an isoelectronic pseudopotential. Specifically, a 10-electron energy-adjusted neon core by Nicklass et al.[101] from the Stuttgart-Dresden pseudopotential library was employed as a coreless pseudopotential with a negative point charge centered at the position of the O nuclei. This eliminates orbital contributions from the bridges while preserving the through-space interaction between the two Cr(III) ions. The BS solutions in the pseudopotential-substituted system converge smoothly and yield reduced values for the exchange coupling constant by ca. 10% for TPSS0, 15% for TPSSh, and 20% for TPSS (computed J values −56.3 cm^{-1}, −72.4 cm^{-1}, and −91.2 cm^{-1}, respectively). Despite the empirical nature of this approach, it can be concluded that ligand-mediated superexchange in the Cr(III) dimer is non-negligible and may account for up to 20% of the total antiferromagnetic coupling.

A fundamentally distinct but complementary approach to the same question is offered by DMRG-driven calculations, which can extend significantly the active space that can be treated by the standard CASSCF calculations described above. The ability to treat large active spaces enables one to study how the computed exchange coupling responds to explicit inclusion of specific orbital sets in the active space−in the present case, of orbitals localized on the bridging ligands. This approach has been suggested in the past[102] and was used in the DMRG framework in the study of the bis-μ-oxo/μ-acetato manganese dimer mentioned above.[61] In that case the metal-only active space DMRG-SCF calculations predicted practically no magnetic coupling. Inclusion of the orbitals of the oxo bridges led to a drastic increase in the magnitude of the exchange coupling from ca. −1 cm^{-1} to almost −60 cm^{-1}, two-thirds of the experimental value, while inclusion of orbitals of the acetato ligand led to no variation in the exchange coupling. These results demonstrated that in the case of the Mn dimer there was no direct metal−metal interaction, that the acetato bridge was not magnetically active, and that antiferromagnetic coupling was exclusively the result of oxo-bridge mediated superexchange.[61]

The same procedure was applied to the present chromium dimer. It is reminded that state-averaged CASSCF calculations with a metal-only (6e,10o) active space led to an exchange coupling constant of −16.8 cm^{-1}. A set of localized OH-bridge orbitals was generated, and the metal-only active space was first expanded by inclusion of O-centered p-type orbitals of the bridges to yield a (24e,19o) active space (Figure 7). State-averaged DMRG-SCF calculations with this active space led to a value of J = −23.9 cm^{-1}. This value is converged at M = 1000, and the relative energies of the four spin states do not deviate from isotropic Heisenberg behavior. Further expansion

DOI: 10.1021/acs.jctc.8b00969
J. Chem. Theory Comput. 2019, 15, 938−948

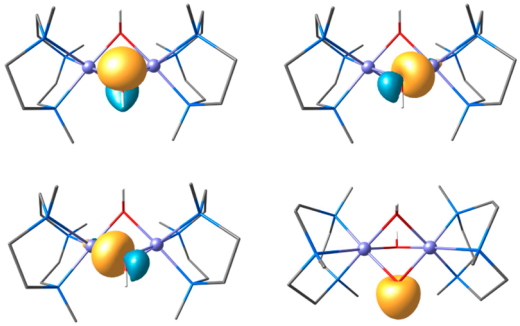

Figure 7. Orbitals localized on the OH bridges (only one bridge is shown as an example), used in the DMRG-SCF calculations with the expanded active spaces (24e,19o) and (30e,22o).

by one additional orbital per bridge of O−H σ-character leads to an active space of (30e,22o). State-averaged DMRG-SCF calculations with this active space (similarly converged at M = 1000 with negligible discarded weights) did not further change the value of J. Not surprisingly, these numbers fall short of the experimental exchange coupling constant because even with a full-valence metal+ligand active space the recovery of dynamic correlation is incomplete.[61] However, the point of interest here is the *relative* contributions from the different orbital subspaces, and in this respect the chromium dimer represents an antithetical situation to the manganese dimer.[61] With reference to the full-valence (30e,22o) DMRG-SCF value of the exchange coupling constant, the bridging orbital subspace in the Cr dimer is a secondary but important contributor to antiferromagnetic coupling, enhancing the metal−metal interaction by less than 30% over the minimal active space result.

The conclusions reached by the DMRG-based active orbital subspace analysis are thus in line with those of the pseudopotential-substitution BS-DFT approach discussed above. While neither of the two approaches demonstrated here can be considered as rigorous or quantitative, through substantially different ways they both converge to the conclusion that antiferromagnetic coupling in the face-sharing Cr(III) dinuclear complex arises primarily through direct metal−metal interaction but also that ligand-mediated superexchange plays a non-negligible ancillary role.

4. CONCLUSIONS

An antiferromagnetically coupled tris-μ-hydroxo Cr(III) dimer, representative of a family of face-sharing d^3−d^3 complexes with intriguing magnetic and spectroscopic properties, was studied with broken-symmetry DFT and multireference CASSCF and DMRG-SCF methods. In contrast to past studies of the same system, it is demonstrated that BS-DFT performs adequately for the problem of the coupling of the two S = 3/2 chromium ions. In tandem with standard spin projection techniques, it predicts correctly the ground spin state of the system and the spacing of the spin ladder, with an optimal percentage of HF exchange similar to that reported for exchange-coupled manganese systems. Past studies of problematic DFT behavior for the chromium dimer were frustrated by intrusion of electronically excited locally low-spin states of the Cr(III) ions in the analysis. The nature of the antiferromagnetic coupling in the chromium dimer was investigated with a variety of methods. Corresponding orbital analysis of the broken-symmetry DFT solutions suggests the dominance of direct metal−metal interaction. This is corroborated by CASSCF calculations which yield significant antiferromagnetic coupling even with a metal-only active space. Two complementary approaches are presented in this study in order to disentangle the contributions of direct exchange and ligand-mediated superexchange. One is based on eliminating superexchange through the bridges by means of pseudopotential substitution in the context of a BS-DFT approach, while the other takes advantage of the access to large active spaces enabled by DMRG to study the effect that specific orbital subspaces have on the spacing of spin states. Both approaches converge to the same conclusion, which represents a more nuanced description of the chromium dimer than the two extremes previously discussed in the literature, namely that the antiferromagnetic coupling is chiefly the result of direct Cr−Cr interaction but that a secondary through-bond superexchange interaction contributes non-negligibly to the stabilization of the antiferromagnetic state.

■ ASSOCIATED CONTENT

Supporting Information

The Supporting Information is available free of charge on the ACS Publications website at DOI: 10.1021/acs.jctc.8b00969.

Tables S1 and S2, Figure S1, and Cartesian coordinates of all structures (PDF)

■ AUTHOR INFORMATION

Corresponding Author

*E-mail: dimitrios.pantazis@kofo.mpg.de.

ORCID

Dimitrios A. Pantazis: 0000-0002-2146-9065

Funding

Support by the Max Planck Society is gratefully acknowledged.

Notes

The author declares no competing financial interest.

■ REFERENCES

(1) Kahn, O. *Molecular Magnetism*; Wiley VCH: New York, 1993; p 396.

(2) de Graaf, C.; Broer, R. *Magnetic Interactions in Molecules and Solids*; Springer: Heidelberg, 2016; p 246, DOI: 10.1007/978-3-319-22951-5.

(3) Malrieu, J. P.; Caballol, R.; Calzado, C. J.; de Graaf, C.; Guihéry, N. Magnetic Interactions in Molecules and Highly Correlated Materials: Physical Content, Analytical Derivation, and Rigorous Extraction of Magnetic Hamiltonians. *Chem. Rev.* **2014**, *114*, 429−492.

(4) Neese, F. Prediction of Molecular Properties and Molecular Spectroscopy with Density Functional Theory: From Fundamental Theory to Exchange-Coupling. *Coord. Chem. Rev.* **2009**, *253*, 526−563.

(5) Anderson, P. W. Antiferromagnetism. Theory of Superexchange Interaction. *Phys. Rev.* **1950**, *79*, 350−356.

(6) Anderson, P. W. New Approach to the Theory of Superexchange Interactions. *Phys. Rev.* **1959**, *115*, 2−13.

(7) Calzado, C. J.; Cabrero, J.; Malrieu, J. P.; Caballol, R. Analysis of the Magnetic Coupling in Binuclear Complexes. I. Physics of the Coupling. *J. Chem. Phys.* **2002**, *116*, 2728−2747.

(8) De Loth, P.; Cassoux, P.; Daudey, J. P.; Malrieu, J. P. Ab Initio Direct Calculation of the Singlet-Triplet Separation in Cupric Acetate Hydrate Dimer. *J. Am. Chem. Soc.* **1981**, *103*, 4007−4016.

(9) Bolster, D. E.; Guetlich, P.; Hatfield, W. E.; Kremer, S.; Mueller, E. W.; Wieghardt, K. Exchange Coupling in Tris(μ-hydroxo)bis-

DOI: 10.1021/acs.jctc.8b00969
J. Chem. Theory Comput. 2019, 15, 938−948

[(1,4,7-trimethyl-1,4,7-triazacyclononane)chromium(III)] Triperchlorate Trihydrate. *Inorg. Chem.* **1983**, *22*, 1725−1729.
(10) Niemann, A.; Bossek, U.; Wieghardt, K.; Butzlaff, C.; Trautwein, A. X.; Nuber, B. A New Structure−Magnetism Relationship for Face-Sharing Transition-Metal Complexes with d^3−d^3 Electronic Configuration. *Angew. Chem., Int. Ed. Engl.* **1992**, *31*, 311−313.
(11) Wieghardt, K.; Chaudhuri, P.; Nuber, B.; Weiss, J. New Triply Hydroxo-Bridged Complexes of Chromium(III), Cobalt(III), and Rhodium(III): Crystal Structure of tris(μ-hydroxo)bis[(1,4,7-trimethyl-1,4,7-triazacyclononane)chromium(III)] Triiodide Trihydrate. *Inorg. Chem.* **1982**, *21*, 3086−3090.
(12) Kremer, S. EPR Spectroscopic Study of *S* = 1, 2, and 3 Spin States of tris(μ-hydroxo)-bridged Chromium(III) Dimers. *Inorg. Chem.* **1985**, *24*, 887−890.
(13) Bennie, S. J.; Collison, D.; McDouall, J. J. W. Electronic and Magnetic Properties of Kremer's tris-Hydroxo Bridged Chromium Dimer: A Challenge for DFT. *J. Chem. Theory Comput.* **2012**, *8*, 4915−4921.
(14) Morsing, T. J.; Weihe, H.; Bendix, J. Probing Effective Hamiltonian Operators by Single-Crystal EPR: A Case Study Using Dinuclear Cr(III) Complexes. *Inorg. Chem.* **2016**, *55*, 1453−1460.
(15) Miralles, J.; Daudey, J.-P.; Caballol, R. Variational Calculation of Small Energy Differences. The Singlet-Triplet Gap in $[Cu_2Cl_6]^{2-}$. *Chem. Phys. Lett.* **1992**, *198*, 555−562.
(16) Miralles, J.; Castell, O.; Caballol, R.; Malrieu, J.-P. Specific CI Calculation of Energy Differences: Transition Energies and Bond Energies. *Chem. Phys.* **1993**, *172*, 33−43.
(17) Calzado, C. J.; Angeli, C.; Taratiel, D.; Caballol, R.; Malrieu, J. P. Analysis of the Magnetic Coupling in Binuclear Systems. III. The Role of the Ligand to Metal Charge Transfer Excitations Revisited. *J. Chem. Phys.* **2009**, *131*, 044327.
(18) Calzado, C. J.; Angeli, C.; Caballol, R.; Malrieu, J.-P. Extending the Active Space in Multireference Configuration Interaction Calculations of Magnetic Coupling Constants. *Theor. Chem. Acc.* **2010**, *126*, 185−196.
(19) Noodleman, L. Valence Bond Description of Anti-ferromagnetic Coupling in Transition-Metal Dimers. *J. Chem. Phys.* **1981**, *74*, 5737−5743.
(20) Noodleman, L.; Davidson, E. R. Ligand Spin Polarization and Antiferromagnetic Coupling in Transition-Metal Dimers. *Chem. Phys.* **1986**, *109*, 131−143.
(21) Yamaguchi, K.; Tsunekawa, T.; Toyoda, Y.; Fueno, T. Ab Initio Molecular Orbital Calculations of Effective Exchange Integrals Between Transition Metal Ions. *Chem. Phys. Lett.* **1988**, *143*, 371−376.
(22) Yamanaka, S.; Kawakami, T.; Nagao, H.; Yamaguchi, K. Effective Exchange Integrals for Open-Shell Species by Density Functional Methods. *Chem. Phys. Lett.* **1994**, *231*, 25−33.
(23) Bencini, A.; Totti, F.; Daul, C. A.; Doclo, K.; Fantucci, P.; Barone, V. Density Functional Calculations of Magnetic Exchange Interactions in Polynuclear Transition Metal Complexes. *Inorg. Chem.* **1997**, *36*, 5022−5030.
(24) Caballol, R.; Castell, O.; Illas, F.; Moreira, I. d. P. R.; Malrieu, J. P. Remarks on the Proper Use of the Broken Symmetry Approach to Magnetic Coupling. *J. Phys. Chem. A* **1997**, *101*, 7860−7866.
(25) Illas, F.; Moreira, I. d. P. R.; de Graaf, C.; Barone, V. Magnetic Coupling in Biradicals, Binuclear Complexes and Wide-Gap Insulators: A Survey of Ab Initio Wave Function and Density Functional Theory Approaches. *Theor. Chem. Acc.* **2000**, *104*, 265−272.
(26) Orio, M.; Pantazis, D. A.; Neese, F. Density Functional Theory. *Photosynth. Res.* **2009**, *102*, 443−453.
(27) Bencini, A.; Totti, F. A Few Comments on the Application of Density Functional Theory to the Calculation of the Magnetic Structure of Oligo-Nuclear Transition Metal Clusters. *J. Chem. Theory Comput.* **2009**, *5*, 144−154.
(28) Peralta, J. E.; Barone, V. Magnetic Exchange Couplings from Noncollinear Spin Density Functional Perturbation Theory. *J. Chem. Phys.* **2008**, *129*, 194107.
(29) Valero, R.; Illas, F.; Truhlar, D. G. Magnetic Coupling in Transition-Metal Binuclear Complexes by Spin-Flip Time-Dependent Density Functional Theory. *J. Chem. Theory Comput.* **2011**, *7*, 3523−3531.
(30) Luo, S.; Rivalta, I.; Batista, V.; Truhlar, D. G. Noncollinear Spins Provide a Self-Consistent Treatment of the Low-Spin State of a Biomimetic Oxomanganese Synthetic Trimer Inspired by the Oxygen Evolving Complex of Photosystem II. *J. Phys. Chem. Lett.* **2011**, *2*, 2629−2633.
(31) Phillips, J. J.; Peralta, J. E. Towards the Blackbox Computation of Magnetic Exchange Coupling Parameters in Polynuclear Transition-Metal Complexes: Theory, Implementation, and Application. *J. Chem. Phys.* **2013**, *138*, 174115.
(32) Steenbock, T.; Tasche, J.; Lichtenstein, A. I.; Herrmann, C. A Green's-Function Approach to Exchange Spin Coupling As a New Tool for Quantum Chemistry. *J. Chem. Theory Comput.* **2015**, *11*, 5651−5664.
(33) Semenaka, V. V.; Nesterova, O. V.; Kokozay, V. N.; Dyakonenko, V. V.; Zubatyuk, R. I.; Shishkin, O. V.; Boča, R.; Jezierska, J.; Ozarowski, A. Cr^{III}−Cr^{III} Interactions in Two Alkoxo-Bridged Heterometallic Zn_2Cr_2 Complexes Self-Assembled from Zinc Oxide, Reinecke's Salt, and Diethanolamine. *Inorg. Chem.* **2010**, *49*, 5460−5471.
(34) Morsing, T. J.; Sauer, S. P. A.; Weihe, H.; Bendix, J.; Døssing, A. Magnetic interactions in oxide-bridged dichromium(III) complexes. Computational determination of the importance of non-bridging ligands. *Inorg. Chim. Acta* **2013**, *396*, 72−77.
(35) Morsing, T. J.; Bendix, J.; Weihe, H.; Døssing, A. Oxo-Bridged Dinuclear Chromium(III) Complexes: Correlation between the Optical and Magnetic Properties and the Basicity of the Oxo Bridge. *Inorg. Chem.* **2014**, *53*, 2996−3003.
(36) Morsing, T. J.; Weihe, H.; Bendix, J. Synthesis, Characterisation and Modelling of a Ferromagnetically Coupled Chromium(III) Dimer: Di-μ-hydroxobis[tetrakis(isothiocyanato)chromate(III)]. *Eur. J. Inorg. Chem.* **2014**, *2014*, 5990−5996.
(37) Sadeghi Googheri, M.; Abolhassani, M. R.; Mirzaei, M. Influence of Ligand-Bridged Substitution on the Exchange Coupling Constant of Chromium-Wheels Host Complexes: a Density Functional Theory Study. *Mol. Phys.* **2018**, *116*, 1306−1319.
(38) Zhao, X. G.; Richardson, W. H.; Chen, J. L.; Li, J.; Noodleman, L.; Tsai, H. L.; Hendrickson, D. N. Density Functional Calculations of Electronic Structure, Charge Distribution, and Spin Coupling in Manganese-Oxo Dimer Complexes. *Inorg. Chem.* **1997**, *36*, 1198−1217.
(39) Petrie, S.; Mukhopadhyay, S.; Armstrong, W. H.; Stranger, R. Theoretical Analysis of the $[Mn_2(\mu\text{-oxo})_2(\mu\text{-carboxylato})_2]^+$ Core. *Phys. Chem. Chem. Phys.* **2004**, *6*, 4871−4877.
(40) Rudberg, E.; Salek, P.; Rinkevicius, Z.; Ågren, H. Heisenberg Exchange in Dinuclear Manganese Complexes: A Density Functional Theory Study. *J. Chem. Theory Comput.* **2006**, *2*, 981−989.
(41) Orio, M.; Pantazis, D. A.; Petrenko, T.; Neese, F. Magnetic and Spectroscopic Properties of Mixed Valence Manganese(III,IV) Dimers: A Systematic Study Using Broken Symmetry Density Functional Theory. *Inorg. Chem.* **2009**, *48*, 7251−7260.
(42) Schinzel, S.; Kaupp, M. Validation of Broken-Symmetry Density Functional Methods for the Calculation of Electron Paramagnetic Resonance Parameters of Dinuclear Mixed-Valence $Mn^{IV}Mn^{III}$ Complexes. *Can. J. Chem.* **2009**, *87*, 1521−1539.
(43) Bovi, D.; Guidoni, L. Magnetic Coupling Constants and Vibrational Frequencies by Extended Broken Symmetry Approach with Hybrid Functionals. *J. Chem. Phys.* **2012**, *137*, 114107.
(44) Krewald, V.; Lassalle-Kaiser, B.; Boron, T. T.; Pollock, C. J.; Kern, J.; Beckwith, M. A.; Yachandra, V. K.; Pecoraro, V. L.; Yano, J.; Neese, F.; DeBeer, S. The Protonation States of Oxo-Bridged Mn^{IV} Dimers Resolved by Experimental and Computational Mn K Pre-

DOI: 10.1021/acs.jctc.8b00969
J. Chem. Theory Comput. 2019, 15, 938−948

Edge X-ray Absorption Spectroscopy. *Inorg. Chem.* **2013**, *52*, 12904−12914.
(45) Baffert, C.; Orio, M.; Pantazis, D. A.; Duboc, C.; Blackman, A. G.; Blondin, G.; Neese, F.; Deronzier, A.; Collomb, M.-N. Trinuclear Terpyridine Frustrated Spin System with a $Mn^{IV}_3O_4$ Core: Synthesis, Physical Characterization, and Quantum Chemical Modeling of Its Magnetic Properties. *Inorg. Chem.* **2009**, *48*, 10281−10288.
(46) Krewald, V.; Neese, F.; Pantazis, D. A. On the Magnetic and Spectroscopic Properties of High-Valent Mn_3CaO_4 Cubanes as Structural Units of Natural and Artificial Water Oxidizing Catalysts. *J. Am. Chem. Soc.* **2013**, *135*, 5726−5739.
(47) Pantazis, D. A.; Orio, M.; Petrenko, T.; Zein, S.; Bill, E.; Lubitz, W.; Messinger, J.; Neese, F. A New Quantum Chemical Approach to the Magnetic Properties of Oligonuclear Transition-Metal Complexes: Application to a Model for the Tetranuclear Manganese Cluster of Photosystem II. *Chem. - Eur. J.* **2009**, *15*, 5108−5123.
(48) Krewald, V.; Retegan, M.; Cox, N.; Messinger, J.; Lubitz, W.; DeBeer, S.; Neese, F.; Pantazis, D. A. Metal Oxidation States in Biological Water Splitting. *Chem. Sci.* **2015**, *6*, 1676−1695.
(49) Shoji, M.; Isobe, H.; Shen, J. R.; Yamaguchi, K. Geometric and Electronic Structures of the Synthetic Mn_4CaO_4 Model Compound Mimicking the Photosynthetic Oxygen-Evolving Complex. *Phys. Chem. Chem. Phys.* **2016**, *18*, 11330−11340.
(50) Paul, S.; Cox, N.; Pantazis, D. A. What Can We Learn from a Biomimetic Model of Nature's Oxygen-Evolving Complex? *Inorg. Chem.* **2017**, *56*, 3875−3888.
(51) Chan, G. K.-L.; Sharma, S. The Density Matrix Renormalization Group in Quantum Chemistry. *Annu. Rev. Phys. Chem.* **2011**, *62*, 465−481.
(52) Marti, K. H.; Reiher, M. New Electron Correlation Theories for Transition Metal Chemistry. *Phys. Chem. Chem. Phys.* **2011**, *13*, 6750−6759.
(53) Olivares-Amaya, R.; Hu, W.; Nakatani, N.; Sharma, S.; Yang, J.; Chan, G. K.-L. The ab-initio Density Matrix Renormalization Group in Practice. *J. Chem. Phys.* **2015**, *142*, 034102.
(54) Yanai, T.; Kurashige, Y.; Mizukami, W.; Chalupský, J.; Lan, T. N.; Saitow, M. Density Matrix Renormalization Group for ab initio Calculations and Associated Dynamic Correlation Methods: A Review of Theory and Applications. *Int. J. Quantum Chem.* **2015**, *115*, 283−299.
(55) Angeli, C.; Cimiraglia, R.; Evangelisti, S.; Leininger, T.; Malrieu, J. P. Introduction of N-Electron Valence States for Multireference Perturbation Theory. *J. Chem. Phys.* **2001**, *114*, 10252−10264.
(56) Angeli, C.; Cimiraglia, R.; Malrieu, J.-P. N-Electron Valence State Perturbation Theory: A Fast Implementation of the Strongly Contracted Variant. *Chem. Phys. Lett.* **2001**, *350*, 297−305.
(57) Angeli, C.; Cimiraglia, R.; Malrieu, J.-P. N-Electron Valence State Perturbation Theory: A Spinless Formulation and an Efficient Implementation of the Strongly Contracted and of the Partially Contracted Variants. *J. Chem. Phys.* **2002**, *117*, 9138−9153.
(58) Guo, S.; Watson, M. A.; Hu, W.; Sun, Q.; Chan, G. K.-L. *N*-Electron Valence State Perturbation Theory Based on a Density Matrix Renormalization Group Reference Function, with Applications to the Chromium Dimer and a Trimer Model of Poly(p-Phenylenevinylene). *J. Chem. Theory Comput.* **2016**, *12*, 1583−1591.
(59) Harris, T. V.; Kurashige, Y.; Yanai, T.; Morokuma, K. Ab initio Density Matrix Renormalization Group Study of Magnetic Coupling in Dinuclear Iron and Chromium Complexes. *J. Chem. Phys.* **2014**, *140*, 054303.
(60) Sharma, S.; Sivalingam, K.; Neese, F.; Chan, G. K.-L. Low-energy Spectrum of Iron−Sulfur Clusters Directly From Many-Particle Quantum Mechanics. *Nat. Chem.* **2014**, *6*, 927−933.
(61) Roemelt, M.; Krewald, V.; Pantazis, D. A. Exchange Coupling Interactions from the Density Matrix Renormalization Group and N-Electron Valence Perturbation Theory: Application to a Biomimetic Mixed-Valence Manganese Complex. *J. Chem. Theory Comput.* **2018**, *14*, 166−179.
(62) Amos, A. T.; Hall, G. G. Single Determinant Wave Functions. *Proc. R. Soc. London, A* **1961**, *263*, 483−493.
(63) Neese, F. Definition of Corresponding Orbitals and the Diradical Character in Broken Symmetry DFT Calculations on Spin Coupled Systems. *J. Phys. Chem. Solids* **2004**, *65*, 781−785.
(64) Tao, J.; Perdew, J. P.; Staroverov, V. N.; Scuseria, G. E. Climbing the Density Functional Ladder: Nonempirical Meta-Generalized Gradient Approximation Designed for Molecules and Solids. *Phys. Rev. Lett.* **2003**, *91*, 146401.
(65) Grimme, S.; Antony, J.; Ehrlich, S.; Krieg, H. A Consistent and Accurate ab initio Parametrization of Density Functional Dispersion Correction (DFT-D) for the 94 Elements H−Pu. *J. Chem. Phys.* **2010**, *132*, 154104.
(66) Grimme, S.; Ehrlich, S.; Goerigk, L. Effect of the Damping Function in Dispersion Corrected Density Functional Theory. *J. Comput. Chem.* **2011**, *32*, 1456−1465.
(67) Weigend, F.; Ahlrichs, R. Balanced Basis Sets of Split Valence, Triple Zeta Valence and Quadruple Zeta Valence Quality for H to Rn: Design and Assessment of Accuracy. *Phys. Chem. Chem. Phys.* **2005**, *7*, 3297−3305.
(68) Weigend, F. Accurate Coulomb-Fitting Basis Sets for H to Rn. *Phys. Chem. Chem. Phys.* **2006**, *8*, 1057−1065.
(69) Neese, F. The ORCA Program System. *WIREs Comput. Mol. Sci.* **2012**, *2*, 73−78.
(70) Neese, F.; Wennmohs, F.; Hansen, A.; Becker, U. Efficient, Approximate and Parallel Hartree−Fock and Hybrid DFT Calculations. A 'Chain-of-Spheres' Algorithm for the Hartree−Fock Exchange. *Chem. Phys.* **2009**, *356*, 98−109.
(71) Yamaguchi, K.; Takahara, Y.; Fueno, T. Ab-Initio Molecular Orbital Studies of Structure and Reactivity of Transition Metal-Oxo Compounds. In *Applied Quantum Chemistry*; Smith, V. H., Jr., Scheafer, H. F., III, Morokuma, K., Eds.; D. Reidel: Boston, 1986; pp 155−184, DOI: 10.1007/978-94-009-4746-7_11.
(72) Chan, G. K.-L.; Head-Gordon, M. Highly Correlated Calculations with a Polynomial Cost Algorithm: A Study of the Density Matrix Renormalization Group. *J. Chem. Phys.* **2002**, *116*, 4462−4476.
(73) Chan, G.; An, K.-L. Algorithm for Large Scale Density Matrix Renormalization Group Calculations. *J. Chem. Phys.* **2004**, *120*, 3172−3178.
(74) Ghosh, D.; Hachmann, J.; Yanai, T.; Chan, G. K.-L. Orbital Optimization in the Density Matrix Renormalization Group, with Applications to Polyenes and *β*-Carotene. *J. Chem. Phys.* **2008**, *128*, 144117.
(75) Sharma, S.; Chan, G. K.-L. Spin-adapted Density Matrix Renormalization Group Algorithms for Quantum Chemistry. *J. Chem. Phys.* **2012**, *136*, 124121.
(76) Neese, F. Importance of Direct Spin-Spin Coupling and Spin-Flip Excitations for the Zero-Field Splittings of Transition Metal Complexes: A Case Study. *J. Am. Chem. Soc.* **2006**, *128*, 10213−10222.
(77) Pipek, J.; Mezey, P. G. A Fast Intrinsic Localization Procedure Applicable for ab initio and Semiempirical Linear Combination of Atomic Orbital Wave Functions. *J. Chem. Phys.* **1989**, *90*, 4916−4926.
(78) Hattig, C. Optimization of Auxiliary Basis Sets for RI-MP2 and RI-CC2 Calculations: Core-Valence and Quintuple-Zeta Basis Sets for H to Ar and QZVPP Basis Sets for Li to Kr. *Phys. Chem. Chem. Phys.* **2005**, *7*, 59−66.
(79) Fiedler, M. A Property of Eigenvectors of Nonnegative Symmetric Matrices and its Application to Graph Theory. *Czech. Math. J.* **1975**, *25*, 619−633.
(80) Fiedler, M. Algebraic Connectivity of Graphs. *Czech. Math. J.* **1973**, *23*, 298−305.
(81) Atkins, J. E.; Boman, E. G.; Hendrickson, B. A Spectral Algorithm for Seriation and the Consecutive Ones Problem. *SIAM J. Comput.* **1998**, *28*, 297−310.
(82) Barcza, G.; Legeza, Ö.; Marti, K. H.; Reiher, M. Quantum-Information Analysis of Electronic States of Different Molecular Structures. *Phys. Rev. A: At., Mol., Opt. Phys.* **2011**, *83*, 012508.

DOI: 10.1021/acs.jctc.8b00969
J. Chem. Theory Comput. 2019, 15, 938−948

(83) Dai, D.; Whangbo, M.-H. Spin Exchange Interactions of a Spin Dimer: Analysis of Broken-Symmetry Spin States in Terms of the Eigenstates of Heisenberg and Ising Spin Hamiltonians. *J. Chem. Phys.* **2003**, *118*, 29−39.
(84) Schreiner, E.; Nair, N. N.; Pollet, R.; Staemmler, V.; Marx, D. Dynamical Magnetostructural Properties of *Anabaena* Ferredoxin. *Proc. Natl. Acad. Sci. U. S. A.* **2007**, *104*, 20725.
(85) Nair, N. N.; Schreiner, E.; Pollet, R.; Staemmler, V.; Marx, D. Magnetostructural Dynamics with the Extended Broken Symmetry Formalism: Antiferromagnetic [2Fe-2S] Complexes. *J. Chem. Theory Comput.* **2008**, *4*, 1174−1188.
(86) Chu, S.; Bovi, D.; Cappelluti, F.; Orellana, A. G.; Martin, H.; Guidoni, L. Effects of Static Correlation between Spin Centers in Multicenter Transition Metal Complexes. *J. Chem. Theory Comput.* **2017**, *13*, 4675−4683.
(87) O'Brien, T. A.; Davidson, E. R. Semiempirical Local Spin: Theory and Implementation of the ZILSH Method for Predicting Heisenberg Exchange Constants of Polynuclear Transition Metal Complexes. *Int. J. Quantum Chem.* **2003**, *92*, 294−325.
(88) Staroverov, V. N.; Scuseria, G. E.; Tao, J.; Perdew, J. P. Comparative Assessment of a New Nonempirical Density Functional: Molecules and Hydrogen-Bonded Complexes. *J. Chem. Phys.* **2003**, *119*, 12129−12137.
(89) Becke, A. D. Density-Functional Thermochemistry.3. The Role Of Exact Exchange. *J. Chem. Phys.* **1993**, *98*, 5648−5652.
(90) Lee, C.; Yang, W.; Parr, R. G. Development of the Colle-Salvetti Correlation-Energy Formula Into a Functional of the Electron-Density. *Phys. Rev. B: Condens. Matter Mater. Phys.* **1988**, *37*, 785−789.
(91) Sproviero, E. M.; Gascon, J. A.; McEvoy, J. P.; Brudvig, G. W.; Batista, V. S. Characterization of Synthetic Oxomanganese Complexes and the Inorganic Core of the O_2-Evolving Complex in Photosystem II: Evaluation of the DFT/B3LYP Level of Theory. *J. Inorg. Biochem.* **2006**, *100*, 786−800.
(92) Mouesca, J. M.; Noodleman, L.; Case, D. A.; Lamotte, B. Spin Densities and Spin Coupling in Iron-Sulfur Clusters: A New Analysis of Hyperfine Coupling Constants. *Inorg. Chem.* **1995**, *34*, 4347−4359.
(93) Sinnecker, S.; Neese, F.; Noodleman, L.; Lubitz, W. Calculating the Electron Paramagnetic Resonance Parameters of Exchange Coupled Transition Metal Complexes Using Broken Symmetry Density Functional Theory: Application to a Mn^{III}/Mn^{IV} Model Compound. *J. Am. Chem. Soc.* **2004**, *126*, 2613−2622.
(94) Sinnecker, S.; Neese, F.; Lubitz, W. Dimanganese Catalase: Spectroscopic Parameters from Broken Symmetry Density Functional Theory of the Superoxidized MnIII/MnIV state. *JBIC, J. Biol. Inorg. Chem.* **2005**, *10*, 231−238.
(95) Kaupp, M.; Bühl, M.; Malkin, V. G. *Calculation of NMR and EPR Parameters: Theory and Applications*; Wiley-VCH: Weinheim, Germany, 2004; p 603, DOI: 10.1002/3527601678.
(96) Schraut, J.; Arbuznikov, A. V.; Schinzel, S.; Kaupp, M. Computation of Hyperfine Tensors for Dinuclear $Mn^{III}Mn^{IV}$ Complexes by Broken-Symmetry Approaches: Anisotropy Transfer Induced by Local Zero-Field Splitting. *ChemPhysChem* **2011**, *12*, 3170−3179.
(97) Spivak, M.; Angeli, C.; Calzado, C. J.; de Graaf, C. Improving the calculation of magnetic coupling constants in MRPT methods. *J. Comput. Chem.* **2014**, *35*, 1665−1671.
(98) Bossek, U.; Saher, M.; Weyhermuller, T.; Wieghardt, K. Asymmetric Mixed Valence Manganese Complexes Containing the $[Mn(\mu\text{-}O)_2(\mu\text{-}MeCo_2)Mn]^{2+}$ Core and their Catalase Reactivity. *J. Chem. Soc., Chem. Commun.* **1992**, 1780−1782.
(99) de Graaf, C.; Sousa, C.; Moreira, I. d. P. R.; Illas, F. Multiconfigurational Perturbation Theory: An Efficient Tool to Predict Magnetic Coupling Parameters in Biradicals, Molecular Complexes, and Ionic Insulators. *J. Phys. Chem. A* **2001**, *105*, 11371−11378.
(100) Muñoz, D.; De Graaf, C.; Illas, F. Putting Error Bars on the *Ab Initio* Theoretical Estimates of the Magnetic Coupling Constants: The Parent Compounds of Superconducting Cuprates as a Case Study. *J. Comput. Chem.* **2004**, *25*, 1234−1241.
(101) Nicklass, A.; Dolg, M.; Stoll, H.; Preuss, H. Ab initio Energy Adjusted Pseudopotentials for the Noble Gases Ne Through Xe: Calculation of Atomic Dipole and Quadrupole Polarizabilities. *J. Chem. Phys.* **1995**, *102*, 8942−8952.
(102) Domingo, A.; Specklin, D.; Rosa, V.; Mameri, S.; Robert, V.; Welter, R. Probing the Influence of the Ligands on the Magnetism of Dinuclear Manganese, Iron, and Chromium Complexes Supported by Aroylhydrazone. *Eur. J. Inorg. Chem.* **2014**, *2014*, 2552−2560.

DOI: 10.1021/acs.jctc.8b00969
J. Chem. Theory Comput. 2019, 15, 938−948